

**Self-Complementary Zwitterionic Peptides Direct Nanoparticle Assembly and Enable Enzymatic Selection of Endocytic Pathways**

*Richard H. Huang, Nazia Nayeem, Ye He, Jorge Morales, Duncan Graham, Rafal Klajn, Maria Contel, Stephen O'Brien, and Rein V. Ulijn\**

R. H. Huang, Dr. Y. He, Prof. R. V. Ulijn  
Advanced Science Research Center at The Graduate Center of the City University of New York, 85 Saint Nicholas Terrace, New York, New York 10031, USA  
E-mail: rulijn@gc.cuny.edu

R. H. Huang, Prof. S. O'Brien  
Department of Chemistry and Biochemistry, The City College of New York, 1024 Marshak, 160 Convent Avenue, NY 10031, USA

R. H. Huang, Prof. M. Contel, Prof. S. O'Brien, Prof. R. V. Ulijn  
Ph.D. Program in Chemistry, The Graduate Center of the City University of New York, 365 Fifth Avenue, New York, New York 10016, USA

N. Nayeem, Prof. M. Contel  
Department of Chemistry, and Brooklyn College Cancer Center, Brooklyn College, The City University of New York, Brooklyn, New York 11210, USA  
Ph.D. Program in Biology, The Graduate Center of the City University of New York, 365 Fifth Avenue, New York, New York 10016, USA

Dr. J. Morales  
Division of Science, The City College of New York, 160 Convent Avenue, NY 10031, USA

Prof. D. Graham  
Centre of Molecular Nanometrology, WestCHEM, Department of Pure and Applied Chemistry, Technology and Innovation Centre, University of Strathclyde, 99 George Street, Glasgow, G1 1RD, UK

Prof. R. Klajn,  
Department of Organic Chemistry, Weizmann Institute of Science, Rehovot 76100, Israel

Prof. R. V. Ulijn  
Department of Chemistry and Biochemistry, Hunter College, The City University of New York, 695 Park Avenue, New York, New York 10065, USA

Keywords: enzyme-responsive materials, MMP, zwitterionic nanoparticles, peptides, self-assembly, cellular uptake, nanomedicine

Abstract: Supramolecular self-assembly in biological systems holds promise as a means to convert and amplify disease-specific signals to physical or mechanical signals that can direct cell fate. The approach requires programmable self-assembling systems that demonstrate tunable and predictable behavior under physiological conditions. Mixed-charge (zwitterionic)

particles are considered suitable for biological applications due to favorable stability. We report on the use of zwitterionic tetrapeptide modalities to direct nanoparticle assembly. These peptides do not form specific folded structures, but they interact through self-complementary patterns of side chain interactions. We demonstrate that the self-assembly can be activated by enzymatic unveiling of zwitterionic LRGD or LRGE modalities through action of matrix metalloprotease-9 (MMP-9), which is over-expressed by cancer cells. Enzymatic activation of gold nanoparticles (AuNPs) decorated with PEGylated peptides ( $[\text{EG}]_8\text{-GPKG}\downarrow\text{LRGD-}[\text{EG}]_5$ ) reveals LRGD sequences that drive multivalent electrostatic assembly of the nanoparticles, giving rise to robust NP assembly. In the vicinity of cancer cells that over-express MMP-9 enzymes, these aggregates form in proximity of these cells and give rise to size-induced selection of cellular uptake mechanism, resulting in diminished cell growth. The enzyme-responsiveness, and therefore indirectly the uptake route, of the system can be programmed by customizing the peptide sequence: a simple inversion of the two amino acids at the cleavage site completely inactivates the enzyme-responsiveness, self-assembly and consequently changes the endocytic pathway. This robust self-complementary, zwitterionic peptide design demonstrates the use of enzyme-activated electrostatic side chain patterns as powerful and customizable peptide modalities to program NP self-assembly and alter cellular response in biological context.

## 1. Introduction

Self-assembly processes in living systems are driven by non-covalent interactions such as hydrogen bonding and electrostatic forces whereby the pattern of interactions further imparts selectivity.<sup>[1,2]</sup> The cooperative use of these relatively weak and reversible interactions has prompted the design of diverse supramolecular architectures that can reorganize upon applied stimuli.<sup>[3,4]</sup> These concepts have been applied in the design of dynamic ligands to create hierarchical superstructures of nanoparticles (NPs) with increasingly sophisticated

architectures.<sup>[5-8]</sup> Particularly, DNA has been a very powerful surface ligand in controlling the aggregation of NPs owing to the specific hydrogen bonding interactions between complementary DNA strands.<sup>[9-12]</sup> Designed peptides potentially provide an even more versatile means of achieving selective assembly of NPs, controlling nanoparticle aggregation due to the vast chemical interaction space that they cover.<sup>[13-23]</sup> Early examples made use of electrostatically induced coiled-coil formation using two<sup>[19]</sup> or three<sup>[20]</sup> component heterogeneous leucine zipper designs. In addition,  $\alpha$ -helical designs could be used to systematically template and control the synthesis and assembly of NPs into helical superstructures.<sup>[21,22]</sup> The disassembly of NPs driven by a change of the surface hydrophobicity has also been demonstrated using a simple ligand comprised of an assembly-directing hydrophobic unit and a disassembly-driving, protease-cleavable short peptide.<sup>[17]</sup>

In a recent study, Stupp and coworkers<sup>[3]</sup> demonstrated the use of charge-complementary peptide sequences as powerful motifs to assemble superstructures by making use of electrostatic side-chain patterns instead of backbone interactions, and these systems demonstrated similar assembly capability to that of DNA. The study used ionic, self-complementary peptides composed of short repeat units of glutamic acid (E) and lysine (K) (separated by a short oligo(ethylene glycol) strand) dictated by complementarity side chain interactions rather than more traditional secondary structure motifs to realize dynamic assembly behavior similar to that achieved with DNA-functionalized structures. The multivalency of the electrostatic interactions in these structures was shown to be crucial in achieving self-assembly and the zwitterionic pattern design not relying on secondary structures holds much promise as a general self-assembly approach. Besides the self-assembly propensity, zwitterions, or mixed charges, have shown benefits in biological context. While negatively charged NPs are known to have low internalization in cells due to electrostatic repulsion with membrane proteins, positively charged NPs can penetrate cellular membranes via strong electrostatic interactions. However, cationic NPs can also attract plasma proteins,

leading to the formation of protein corona that potentially changes the biological identity of the NPs.<sup>[24,25]</sup> By contrast, pH-sensitive zwitterionic NPs have been demonstrated to effectively penetrate and kill cancer cells while providing the unreactive “stealth” surface. <sup>[26–28]</sup>

NPs and their assemblies have been actively used in biomedical applications such as biosensing, imaging and detection.<sup>[29–34]</sup> Recent studies have focused on the development of NP systems that can be activated *in situ* by exploring specific features of a diseased state environment and that give rise to mechanical or physical changes that cells respond to, for example through localized aggregation, size dependent uptake or clearance. One attractive stimulus in this context is disease-related enzymes that are often over-expressed and hence subject to be targets for specific substrates. For example, solid tumor tissues have specific physiological characteristics differing from healthy tissues, such as the over-expression of matrix metalloproteinases (MMPs) in the extracellular matrix<sup>[35,36]</sup> As a result, MMP-triggered peptide cleavage systems have achieved success in both cancer cell destruction and/or the detection of specific disease states in cancer progression.<sup>[18,35,37]</sup> Moreover, studies have designed systems that incorporate both an MMP-cleavable peptide and a fibronectin-derived cell adhesive moiety, RGD, within the peptide sequence that simultaneously target MMPs and overexpressed integrin receptors.<sup>[38,39]</sup>

Here, we demonstrate a robust and simple platform for triggered nanoparticle assembly based on zwitterionic peptide modalities that undergo powerful assembly in aqueous media of cellular environments and demonstrate its ability to direct cell fate (**Figure 1**). We first demonstrate that gold nanoparticles (AuNPs) functionalized with PEGylated peptides GPKG↓LRGD (↓ indicates cleavage site) exhibit switch like response to MMP-9 (Figure 1A). The LRGD motif, originally designed as a cell adhesive ligand, was serendipitously discovered to act as a minimalistic version of the charge-complementary sequence developed by Stupp and coworkers,<sup>[3]</sup> which drives the assembly of the AuNPs via multivalent

electrostatic bindings after MMP-9-triggered peptide cleavage. By a simple inversion of the amino acids at the cleavage site, the MMP-9 responsiveness of the peptide-NP conjugates is completely shut down, causing drastic changes in cellular uptake mechanism and subsequent cell behavior (Figure 1B). Overall, our results demonstrate the use of enzyme-activated, minimalistic electrostatic patterns in short peptide ligands to effectively trigger the self-assembly of NPs in biological contexts and alter the entry of these NPs into target cells.

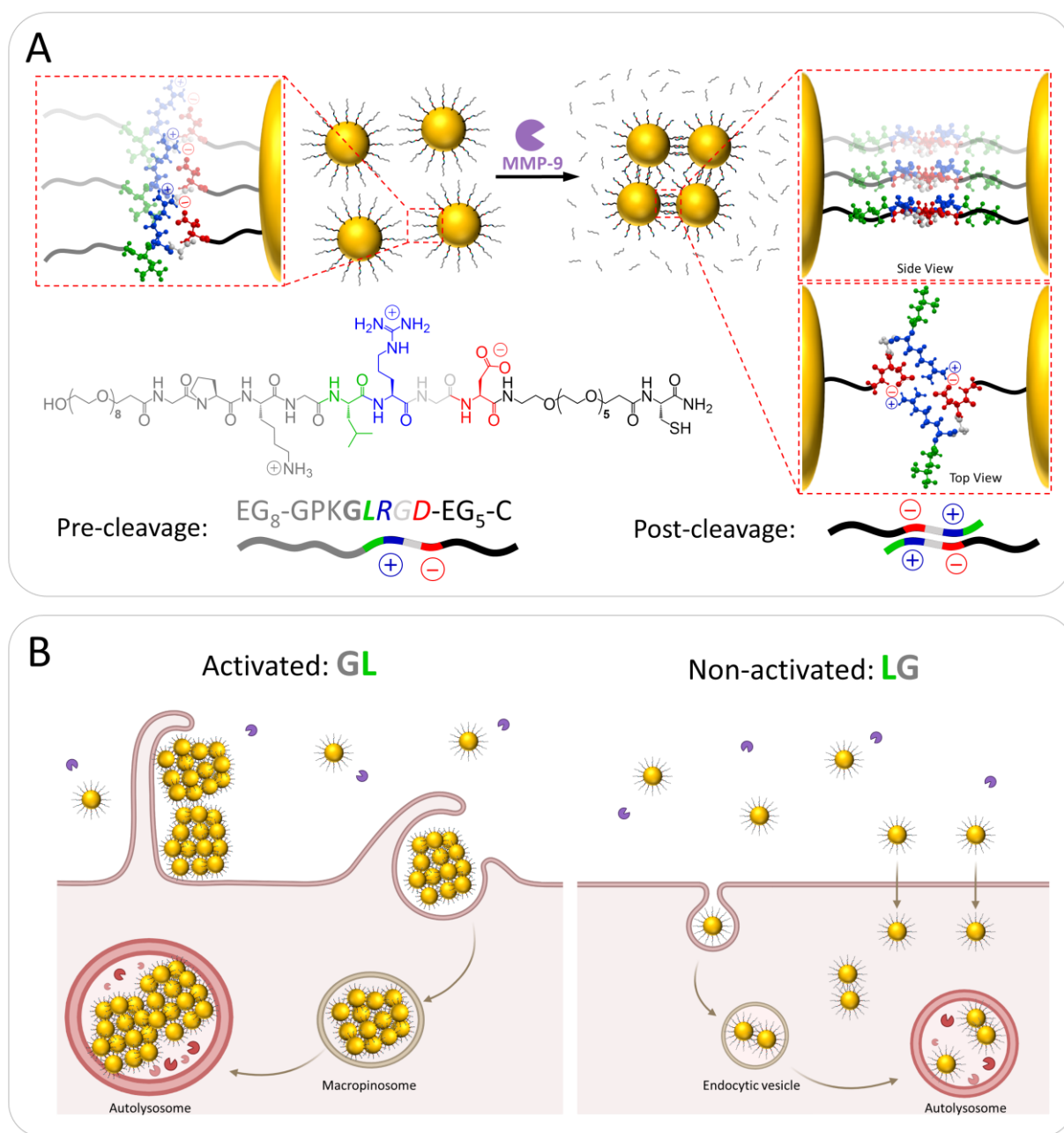


**Figure 1.** Summary of enzyme-responsive nanoparticle system for controlled endocytic pathways. (A) Schematic illustration of MMP-9-triggered assembly of AuNPs using charge-

complementary peptides. The structural formula, pre-cleavage, and post-cleavage cartoon representations of MMP-9 responsive peptide ligand, [EG]<sub>8</sub>-GPKG↓LRGD-[EG]<sub>5</sub>-C, are shown. (B) Schematic illustration of distinct endocytic pathways of the NPs due to enzyme responsiveness. When the cleavage site is Gly-Leu, the ligand can be cleaved by MMP-9 (“activated”). When the cleavage site is Leu-Gly, the ligand cannot be cleaved by MMP-9 (“non-activated”). The activated AuNPs form aggregates and undergo macropinocytosis. The non-activated AuNPs remain discrete and undergo pinocytosis or direct membrane penetration.

## 2. Results and Discussion

### 2.1. Design of MMP-9 responsive peptide ligands

We designed four PEGylated peptide sequences – GPKGLRGD (**GLD**), GPKGLRGE (**GLE**), GPKLGRGD (**LGD**) and GPKLGRGE (**LGE**) (**Table 1**) to illustrate the enzymatic specificity of MMP-9 and to further prepare peptide–gold conjugates. The rationale behind the design of these ligands is as follows: (a) **GLD** and **GLE** are expected to be cleaved by MMP-9,<sup>[40]</sup> at the GX (P<sub>1</sub>↓P<sub>1</sub>') position (Table 1), where X should have a small hydrophobic side chain (*i.e.*, A, V, L, or I); (b) after a simple inversion of the GL sequence, **LGD** and **LGE** may serve as negative controls: MMP-9 is not expected to hydrolyze the LG sequence at the P<sub>1</sub>↓P<sub>1</sub>' site or the GR sequence at the P<sub>1</sub>'↓P<sub>2</sub>' site; (c) all peptides have a net positive charge to electrostatically attract MMP-9 to ensure enhanced activity (pI = 5.7, net negative charge at physiological pH);<sup>[41,42]</sup> (d) the OEG at the N-terminus of the peptide provides colloidal stability for the AuNP at physiological salt concentration; (e) the OEG at the C-terminus of the peptide adds distance and reduces steric hindrance between the peptide and the AuNP surface, ultimately improving the accessibility of MMP-9; (f) the terminal cysteine residue facilitates the immobilization of the peptide ligand to the AuNP surface *via* thiol–gold binding;<sup>[43,44]</sup> and (g) the RGD sequence plays a dual role of promoting AuNP aggregation

after peptide cleavage *via* electrostatic interaction and potentially binding to the cancer cell membranes that overexpress  $\alpha_v\beta_3$  integrin receptors,<sup>[45,46]</sup> whereas the RGE sequence serves as an integrin-inactive control.<sup>[47]</sup> The peptide ligands were synthesized using Fmoc-based solid-phase peptide synthesis (SPPS), PEGylated, purified on preparative high-performance liquid chromatography (HPLC), lyophilized in water, and characterized by liquid chromatography–mass spectrometry (LCMS). The chemical structures and LCMS spectra of the peptide ligands are shown in Figure S1, Supporting Information.

We measured the rate of peptide hydrolysis by MMP-9, firstly in the absence of AuNPs to facilitate direct analysis by LCMS. Lyophilized peptide ligands were dissolved in phosphate-buffered saline (PBS) buffer at pH 7.4, supplemented with  $\text{CaCl}_2$  and  $\text{ZnCl}_2$  for compatibility with MMP-9 (a metalloproteinase with zinc- and calcium-dependent catalytic domain), and sonicated for 10 min to achieve 1 mM peptide solutions. Then, 100 ng/mL MMP-9 was incubated with the peptides at 37 °C, and the reaction was monitored up to 48 hours using LCMS to identify and quantify the enzymatic products. As shown in **Figure 2A**, over 96% of **GLD** and **GLE** was cleaved by MMP-9 in 48 hours. The enzymatic products were characterized and confirmed by LCMS; as expected, the cleavage site occurred at G↓L (Figure S2 A and B, Supporting Information). In contrast, we did not observe the formation of enzymatic products from **LGD** or **LGE** over 48 hours (Figure S2 C and D, Supporting Information). Such drastic change in enzyme responsiveness demonstrated a high specificity of MMP-9 to the GL sequence at the  $\text{P}_1\downarrow\text{P}_1'$  site. The overall positive charge of the peptides could be vital in achieving the cleavage at one unique position; it has been reported that negatively charged peptides with similar lengths exhibited inconsistent cleavage sites ( $\text{P}_6\downarrow\text{P}_5$ ,  $\text{P}_2\downarrow\text{P}_1$ , or  $\text{P}_1'\downarrow\text{P}_2'$ ) by MMP-9 under the same experimental conditions.<sup>[42,48]</sup> To the best of our knowledge, this level of selectivity with such minimal change in sequence by design has not been demonstrated before in MMP-responsive materials.

**Table 1.** Design of peptide ligands (red dashed line indicates the cleavage site) and their expected responsiveness to MMP-9.

Code	Peptide Sequence											MMP-9 responsive
	P <sub>4</sub>	P <sub>3</sub>	P <sub>2</sub>	P <sub>1</sub>	P <sub>1</sub> '	P <sub>2</sub> '	P <sub>3</sub> '	P <sub>4</sub> '	Anchor			
				X <sub>1</sub>	X <sub>2</sub>							
<b>GLD</b>	EG <sub>8</sub>	G	P	K	G	L	R	G	D	EG <sub>5</sub>	C	Yes
<b>GLE</b>	EG <sub>8</sub>	G	P	K	G	L	R	G	E	EG <sub>5</sub>	C	Yes
<b>LGD</b>	EG <sub>8</sub>	G	P	K	L	G	R	G	D	EG <sub>5</sub>	C	No
<b>LGE</b>	EG <sub>8</sub>	G	P	K	L	G	R	G	E	EG <sub>5</sub>	C	No

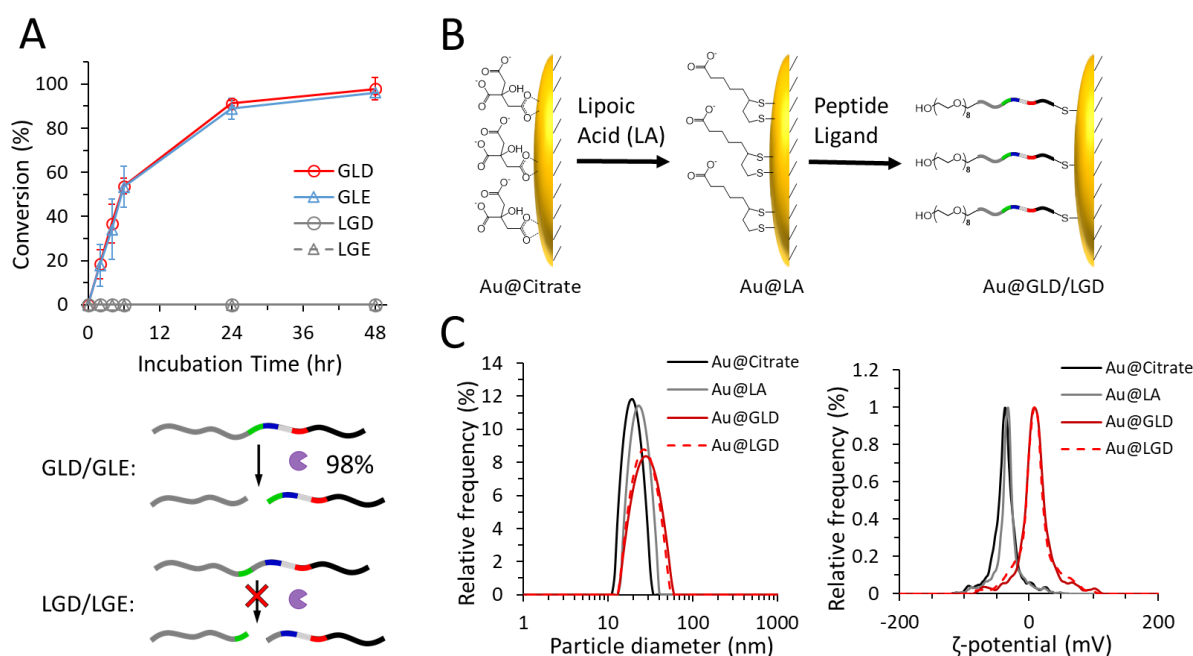


**Figure 2.** (A) MMP-9 specificity measured by LC–MS. Peptide ligands **GLD**, **GLE**, **LGD**, and **LGE** (1 mM) were incubated with 100 ng/mL of MMP-9 at 37°C. Percentage conversion of the peptides to the enzymatic products are shown. These results confirm that MMP-9 is highly specific to the **GLD/GLE** ligand at the P<sub>1</sub>↓P<sub>1</sub>' site. Error bars, mean ± SD (n = 2). (B) Schematic illustration of the two-step synthesis of peptide–AuNP conjugates. First, citrate-stabilized AuNPs<sup>[61]</sup> were treated with an excess of α-lipoic acid (LA) to replace the citrate molecules and block the gold surface to prevent non-thiol–gold interactions. Then, excess of peptides was added to allow a second ligand exchange to allow for peptide–AuNP

conjugation. The schematic represents an idealized situation of a quantitative ligand exchange at each step. (C) Hydrodynamic size measurements by DLS (left) and  $\zeta$ -potential measurements (right) of the AuNPs at each step of the surface immobilization process.

## 2.2. Immobilization of peptide ligands on NPs

The surface functionalization of  $16.5 \pm 0.5$  nm spherical AuNPs with the peptide ligands was achieved by a two-step ligand exchange process starting from AuNPs prepared by the citrate reduction method. The morphology, particle size, and  $\zeta$ -potential of the as-synthesized citrate-stabilized AuNPs (Au@Citrate) are shown in Supporting Information (Figure S3). A schematic illustration of the ligand exchange process is shown in Figure 2B. Alpha-lipoic acid (LA) was used as an intermediate ligand to block the gold surface and to prevent any non-thiol–gold interactions. LA was previously shown to be particularly effective as an intermediate ligand for AuNPs prior to the subsequent coupling of positively charged peptides.<sup>[49]</sup> This was indeed found to be a crucial step to prevent AuNP aggregation upon peptide addition: without the intermediate ligand, both the amine group of the lysine residue and the thiol group of the cysteine residue on the peptide ligands are able to bind to the gold surface and consequently promote crosslinking of the particles.<sup>[50–52]</sup> The LA intermediate ligands on the surface prevent undesired amine–gold interaction and favor the stronger thiol–gold binding between the peptide ligands and the AuNPs. Successful coupling of LA to the surface of AuNPs was evidenced by the stability of Au@LA at physiological salt concentration, whereas Au@Citrate NPs aggregated immediately upon addition of TBS buffer (Figure S4, Supporting Information). In the second step, a 10-fold excess of peptides (relative to the amount of LA immobilized on the AuNPs, assuming a grafting density<sup>[53]</sup> of 4 molecules/nm<sup>2</sup>) was used to competitively drive the displacement of the LA. As such, this step required a longer reaction time of up to 24 hours. The peptide–NP conjugation was monitored and confirmed by  $\zeta$ -potential measurements until the positive value of  $\zeta$ -potential

plateaued. The increasing hydrodynamic diameters and the change of  $\zeta$ -potentials of the NPs at each step are shown in Figure 2C. To further confirm that the peptide ligands were bound directly to the surface of the AuNPs (and not electrostatically adsorbed to the LA ligands), the stability of NPs was monitored by lowering the pH to 2 by adding HCl. It can be expected that if the dominant ligand on the AuNP surface is LA, the protonated carboxylates would drive the aggregation of the NPs. However, we observed that the NPs retained colloidal stability (*i.e.*, the wine-red color was retained) at pH 2; although we cannot exclude the presence of residual lipoic acid on the surface of the NPs, our results suggest that the dominant ligands on the AuNPs are the PEGylated peptide ligands.

### **2.3. Enzyme-activated aggregation of NPs driven by charge-complementary peptide ligands**

To investigate the specificity of MMP-9 on the immobilized peptides on AuNPs, Au@GLD, Au@GLE, Au@LGD, and Au@LGE were incubated with MMP-9 for up to 48 hours. The color of the solution, the particle size, and the  $\zeta$ -potential were monitored over time. **Figure 3A** shows that the characteristic red color of the AuNPs in the Au@GLD and Au@GLE solutions turned purple within the first hour. This result indicates that the particles started to aggregate when only limited amount of the peptides were cleaved, given that the hydrolysis of the immobilized peptides by MMP-9 is likely slower<sup>[54]</sup> than that of the free peptides (<10% at  $t = 1$  hour, Figure 2A). The color of the solution gradually disappeared as the particles continued to aggregate and settle. For Au@GLD and Au@GLE, all the particles settled within 6 hours of incubation with MMP-9 (Figure 3A). At 6 hours, 40-48% of peptides were cleaved by MMP-9 when the peptides were not immobilized (Figure 2A). Such an early onset of NP aggregation was expected because the aggregation could occur as long as a sufficient fraction of peptides was cleaved to expose the RGD sequence that drove multivalent electrostatic interaction. This level of aggregation is much more significant compared to many

DNA- or peptide-based systems where a more subtle red-shift of the LSPR band is commonly observed.<sup>[10,14]</sup> By increasing the acidity of the solution to pH 2, the aggregated AuNPs at 48 hours became dispersed again, as manifested by the reappearance of the wine-red color, indicating that the aggregation was indeed driven by electrostatic interactions between the RGD moieties on the AuNPs.  $\zeta$ -potential measurements of the Au@GLD and Au@GLE particles showed a shift of the surface charge from positive (+12 mV) to negative (−8 mV), indicating that the aggregated particles had a weakly negatively charged surface after the GLD peptides were cleaved (Figure 3C). We propose that the L residue which remains upon enzymatic cleavage further enhances the electrostatic interactions by providing an apolar environment which shields the ionic bonds. TEM images and hydrodynamic size measurements by DLS at 48 hours after MMP-9 incubation also confirmed that the Au@GLD and Au@GLE particles formed aggregates at  $585 \pm 19$  nm and  $630 \pm 8$  nm, respectively (Figure 3D, and S5, Supporting Information). In the case of Au@LGD and Au@LGE, the color of the solution, particle size, and  $\zeta$ -potential remained unchanged after MMP-9 incubation, as anticipated.

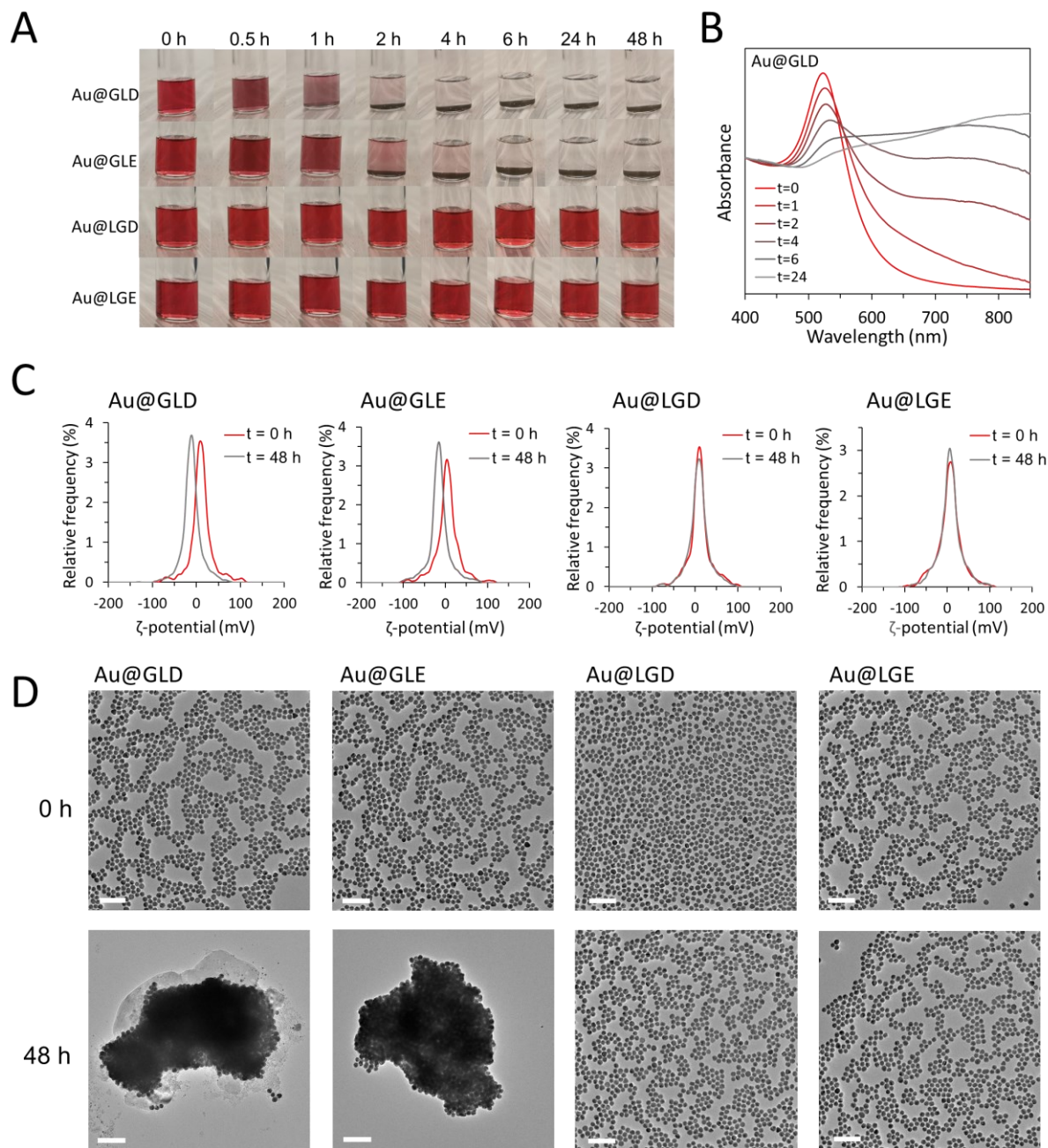


**Figure 3.** MMP-9-triggered AuNP aggregation. (A) Photographs of peptide-functionalized nanoparticles, Au@GLD, Au@GLE, Au@LGD, and Au@LGE incubated with MMP-9 at 37 °C and pH 7.4 over 48 hours. For Au@GLD and Au@GLE, the characteristic red color of the solution turned purple and then colorless, indicating that the AuNPs aggregated and then settled over time. For Au@LGD and Au@LGE, the peptides were not cleaved by MMP-9 and thus the particles remained stable. (B) UV-Vis spectra of the Au@GLD NPs incubated with MMP-9 over time. (C)  $\zeta$ -potential measurements of the peptide-functionalized NPs at 0

and 48 hours following the incubation of MMP-9. The Au@GLD and Au@LGE NPs showed a shift of the surface charge from positive to negative, indicating that the aggregated particles had an overall negatively charged surface after the peptide ligands were cleaved. (D) TEM images confirmed that the Au@GLD and Au@GLE particles aggregated at 48 hours while the Au@LGD and Au@LGE particles remained discrete. Scale bars, 100 nm.

Notably, AuNPs functionalized with the same peptide appended with longer PEG chains ( $M_n = 2000$ ; ~45 ethylene glycol units) aggregated much slower (Figure S6, Supporting Information), suggesting that the longer PEG chains hindered the access of MMP-9 to the peptide cleavage site, hence slowing down the cleavage reaction. This observation is consistent with previously reported system using PEG-2000-terminated peptides immobilized on glass surfaces showing reduced enzymatic conversions.<sup>[55]</sup> We reiterate here that the EG<sub>8</sub> linker used in our system does not compromise the recognition of the peptide sequence by MMP-9 while providing sufficient colloidal stability for the AuNPs.

#### 2.4. MMP-9-responsive NPs slow down cancer cell growth

To evaluate the effects of the MMP-9-responsive NPs on cells, cell viability assays were performed using MDA-MB-231, a metastatic triple negative breast cancer cell line, versus IMR-90 normal lung fibroblast cells. Expressions of MMP-9 and integrin are both promoted in metastatic breast cancer cells as these two factors cooperate to enhance breast cancer cell migration which requires degradation of the local extracellular matrix.<sup>[45]</sup> **Figure 4A** shows that the incubation of cancer cells with MMP-9-responsive NPs, Au@GLD and Au@GLE, for 48 hours resulted in a significant decrease in cell viability in comparison to the controls where no NPs were added. Cancer cells treated with NPs not responsive to MMP-9, Au@LGD and Au@LGE, also exhibited reduced viability but to a significantly lesser extent, and this was observed across all the NP concentrations tested. In contrast, the influence of both MMP-9-responsive and non-responsive NPs on the cell viability of non-tumor cells was

marginal (Figure 4B). The cell viabilities of both cell lines were also measured at 24- and 72-hours following incubation with the peptide-functionalized NPs (Figure S7, Supporting Information). The cell viabilities for the non-tumor cells were consistent throughout all 3 time points as expected. For the cancer cells, a decrease in cell viabilities among all NPs was observed from 24 to 48 hours. However, an increase of cell viabilities was observed at 72 hours of incubation, likely due to cell recovery and continued proliferation of unaffected cells between 48 to 72 hours. Interestingly, there was no significant difference in viability between the cancer cells treated with the RGD-containing NPs and those treated with the RGE-containing NPs. The comparable cancer cell response to the NPs aggregates may relate to formation of protein corona<sup>[24]</sup> on the surface of the NP aggregates, which could also cause the cells to treat the NPs indifferently.

## **2.5. The effect of MMP-9 responsiveness of the NPs on cellular uptake and endocytic pathways**

Two scenarios could cause the difference in cell viability between the cancer cells treated with MMP-9-responsive and non-responsive NPs: first, the aggregates formed by the MMP-9-responsive NPs were internalized while the non-responsive NPs were not; second, internalization occurred for both types of NPs, but their respective internalizing pathways and biodistributions differed significantly. To evaluate this, we employed confocal reflection microscopy to track the biodistribution of NPs and TEM to obtain the precise locations of the NPs in cells. Confocal reflection imaging revealed that NP aggregates can be clearly observed inside MDA-MB-231 triple negative breast cancer cells and are co-localized with endosomes and/or lysosomes (Figure 4C). In contrast, no signs of NP aggregates can be detected in non-tumor cells (Figure 4D). In addition to NP aggregation, the elevated endocytic activity in cancer cells due to the dysregulation of endocytic proteins might have also contributed to the difference in cytotoxicity between the two cell lines. Importantly, the largest aggregates were

observed in cancer cells treated with the Au@GLD NPs, while the Au@GLE NPs formed smaller aggregates. The non-MMP-responsive NPs Au@LGD and Au@LGE unexpectedly formed aggregates in cancer cells, suggesting a different mechanism that drove the assembly of the NPs. The combined observations that both the MMP-9-responsive and non-responsive NPs were internalized in cancer cells and that the MMP-9-responsive NPs resulted in significantly lower cell viability suggest that there is a key difference in cellular uptake mechanisms between the two types of NPs. Thus, we further employed TEM to examine the NPs at the sub-cellular level in cancer cells. The TEM images in Figure 4E revealed that the Au@GLD NPs formed large aggregates outside of the cell and these were internalized via macropinocytosis,<sup>[56,57]</sup> an actin-dependent endocytic pathway that cells undergo to capture foreign objects in the size range of 100-1000 nm. In contrast, being unable to form large aggregates due to lack of MMP-9 responsiveness, the Au@LGD NPs were internalized by receptor-mediated endocytosis, as observed by the small vesicles capturing individual NPs or small clumps thereof (Figure 4E and Figure S8, Supporting Information). Additionally, some of the Au@LGD NPs can be found in cytoplasm without being encapsulated by vesicles (Figure S8, Supporting Information), indicating that direct membrane penetration of these NPs also occurred, possibly due to the positive charge of the peptide ligands. We propose that this distinct difference in endocytic pathways is likely the cause of the difference in cell viabilities between the MMP-9-responsive and non-responsive NPs: macropinocytosis requires the formation and assembly of actin, which serves as the scaffolding for membrane ruffling; the large energy cost in this active process resulted in the slower growth of the cells. Previous real-time studies have shown that the process of macropinocytosis from the formation of membrane ruffling to the complete development of macropinosome can take up to 10 minutes, while the time it takes for clathrin-mediated endocytosis is within seconds in comparison.<sup>[58,59]</sup>

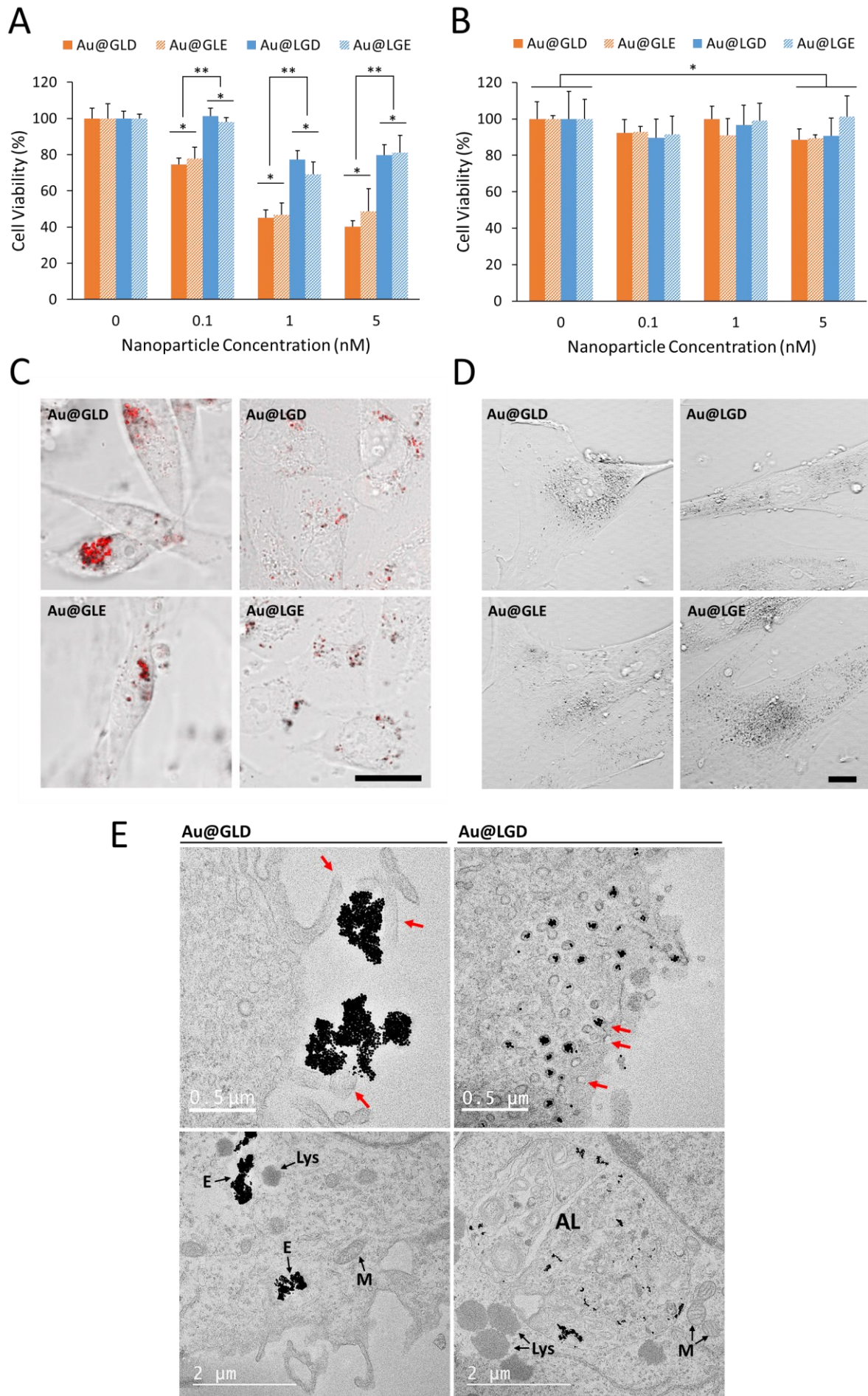


**Figure 4.** Impact of MMP-9 responsive and non-responsive NPs on cells. (A, B) Cell viability of MDA-MB-231 triple negative breast cancer cells and IMR-90 normal lung fibroblast cells using PrestoBlue assay following 48 hours of incubation with NPs at different concentrations. Error bars, mean  $\pm$  SD ( $3 \leq n \leq 6$ ). \* $P > 0.05$ , \*\* $P < 0.001$ , statistics by one way ANOVA. (C, D) Confocal images of MDA-MB-231 cancer cells and IMR-90 cells treated with the indicated NPs for 48 hours. AuNP aggregates (red) were visualized in confocal reflection mode. Scale bars, 20  $\mu\text{m}$ . (E) TEM images of MDA-MB-231 cancer cells treated with Au@GLD and Au@LGD. Red arrows indicate the distinct features of macropinocytosis (left) versus receptor mediated endocytosis (right). E: endosome; M: mitochondria; Lys: lysosome; AL: autolysosome.

### 3. Conclusion

In summary, we present the modular design of an enzyme-activated AuNP aggregation system using immobilized MMP-9-cleavable peptides which reveal LRGD as a self-complementary assembly motif and a potential cell adhesive ligand (or LRGE as a self-assembling, non-cell-adhesive control). We show that the assembly of peptide-functionalized AuNPs *via* electrostatic complementarity can be achieved using the minimalistic peptide sequence LRGD – an approach that is expected to be generally applicable for supramolecular self-assembly driven by a self-complementary ligand that can potentially be expanded to different charge patterns to give rise to selectivity. In addition, we demonstrate that this MMP-triggered, electrostatically driven assembly of NP is programmable by changing the peptide sequence, i.e., as simple as swapping the amino acids at the P1/P1' position. With this level of specificity, our modular NP system shows potential biosensing capabilities that take advantage of enzyme specificity and amplification and may be extended to other cancer-targeting drug delivery systems. When the NPs are exposed to triple negative breast cancer cells with high MMP-9 expression level versus normal cells, distinct cellular responses are

observed. Furthermore, we demonstrate that the programmable assembly of the NPs alters endocytic pathways and reduces cancer cell viability.

Overall, the NP platform in this study offers the ability to direct cellular uptake pathways and consequently influence cancer cell growth using zwitterionic self-assembling peptides. With the selective cytotoxicity demonstrated, the enzyme-mediated NP aggregation design holds potential for cancer therapy via physical damage/interruption of cells without the need for incorporating anti-cancer drugs. The level of cytotoxicity (up to 60%) is comparable to previous study that used a combination of enzyme-induced AuNP assembly and photothermal therapy at equivalent concentration of NPs.<sup>[60]</sup> The MMP-responsive AuNP aggregates may also serve as a signal amplification system for cancer targeting computed tomography (CT) or surface-enhanced Raman spectroscopy (SERS) imaging,<sup>[61–63]</sup> piezoelectric or electric biosensors owing to the mass and charge stored in the NP aggregates,<sup>[64]</sup> or protease biosensor for the rapid detection of SARS-Cov-2.<sup>[65]</sup> These areas will be subject of further study.

#### 4. Experimental Section

*Synthesis of Peptide Ligands:* Peptide fragments in **GLD**, **GLE**, **LGD**, and **LGE** without the N-terminal OEG chains were synthesized on a CEM Liberty Blue microwave-assisted solid-phase peptide synthesizer (USA) using Rink Amide resin and Fmoc-protected amino acids in 1:6 resin to amino acid ratio (double coupling for lysine and single coupling for all other amino acids). The C-terminal OEG was coupled using Fmoc-(EG)<sub>5</sub>-CH<sub>2</sub>CH<sub>2</sub>COOH (Sigma-Aldrich) within the synthesizer. The complete peptide-loaded resins (without the N-terminal OEG chains) were washed three times in dichloromethane on a filtration column. Then, the N-terminal OEG was coupled to the peptide using HO-(EG)<sub>8</sub>-CH<sub>2</sub>CH<sub>2</sub>COOH (Sigma-Aldrich) (3-fold excess over the resin). N,N,N',N'-tetramethyl-O-(1H-benzotriazol-1-yl)uronium hexafluorophosphate (HBTU) and N-ethyl-N,N-diisopropylamine (DIPEA) were used as the activating and coupling reagents in 1:2, respectively, relative to the OEG molecule.

Finally, the resins and side chain protecting groups were removed from the peptides by treatment with a TFA cocktail (92.5% TFA, 2.5% triisopropylsilane, 2.5% 2,2'-(ethylenedioxy)diethanethiol, and 2.5% water) for 4 h. The complete peptide ligands were recovered by removing the TFA cocktail, followed by precipitation in cold diethyl ether. The peptide ligands were washed three times in ice cold diethyl ether using a centrifuge to decant the supernatant. The crude peptide ligands were purified by preparative HPLC using a C<sub>18</sub> column (100x21 mm, 5 μm, flow rate at 8 mL/min) on a Thermo Scientific Dionex Ultimate 3000. To remove the residual TFA salts attached to the amino groups,<sup>[66]</sup> the peptide ligands were dissolved in HCl solutions (1 mg/mL of peptide ligand in 10 mM HCl) to allow for anion exchange. The solution was then lyophilized overnight to remove all liquid. The HCl wash/lyophilization cycle was repeated two more times and the peptide ligands were finally lyophilized in Milli-Q water. The purified and TFA-removed peptide ligands were characterized by LCMS (Figure S1).

*Peptide Cleavage by MMP-9:* MMP-9 (catalytic domain, human) (recombinant, *E. coli*) was purchased from Enzo. The purchased enzyme solution was defrosted and aliquots were made for storage at -80 °C. The 1 mM peptides were prepared in PBS (2.7 mM KCl, 137 mM NaCl, supplemented with 1 mM CaCl<sub>2</sub> and 55 μM ZnCl<sub>2</sub>), and the pH was adjusted to 7.4 using 0.5 M NaOH or HCl. Then, 1 mL of peptide solution was then incubated at 37 °C in a stationary heat block with 100 ng/mL ( $2.56 \cdot 10^{-9}$  mol/L) of MMP-9. Reaction samples (50 μL) were taken at each time point (Figure 2) for up to 48 h for LCMS analysis.

*Synthesis of Gold Nanoparticles:* The preparation of monodisperse spherical AuNPs followed the standard citrate reduction method<sup>[67,68]</sup> with some modifications. Briefly, a solution of 100 mL of 0.5 mM HAuCl<sub>4</sub> was prepared. The pH of the solution was adjusted to approximately 4.0 using 1 M NaOH solution. The mixture was heated to boil in a round-bottom flask equipped with a condenser. Then, 0.39 mL of 0.5 M sodium citrate solution was added quickly. The reaction mixture was refluxed under magnetic stirring for 30-40 minutes until a

characteristic wine-red color was observed. This method produced highly monodisperse (PDI ~5%) gold nanoparticles with an average diameter of 16 nm (TEM).

*Peptide Immobilization on Gold Nanoparticles:* The NP-peptide coupling was achieved through a two-step coupling process using  $\alpha$ -lipoic acid (LA) as an intermediate ligand.<sup>[47]</sup> The as-synthesized gold nanoparticles were centrifuged at 13,500 RPM and subsequently redispersed in sodium phosphate buffer (10 mM, pH 7.4) to a concentration where the optical density (OD) is 1. In the first step, 5 mL of the above AuNP solution was incubated overnight with 20  $\mu$ L of LA (10 mM in ethanol) under gentle agitation. The LA-functionalized AuNPs (Au@LA) were then centrifuged at 13,500 RPM for 10 minutes, followed by decantation of supernatant. The Au@LA NPs were re-dispersed in water, and the centrifugation/wash cycle was repeated two more times. In the second step, 5 mL of the purified Au@LA NPs in phosphate buffer (10 mM, pH 7.4) was incubated with 400  $\mu$ L of the respective peptide ligands (1 mM in phosphate buffer) for 24 h under gentle agitation. The number of peptide ligands added was approximately 10 times that of the immobilized LA on the AuNP, assuming a grafting density of 4 molecules/nm<sup>2</sup>. Tween 20 was added to this solution (final concentration = 0.05% v/v) to avoid non-specific binding of the peptides. Excess peptides were removed by three centrifugation/wash cycles (13,500 RPM for 10 minutes using water). The purified Au@peptide NPs (Au@GLD, Au@GLE, Au@LGD, and Au@LGE) were re-dispersed in 5 mL of 1 $\times$  PBS at pH 7.4.

*Cell Lines:* Human breast adenocarcinoma MDA-MB-231 and lung fibroblast IMR-90 lines were obtained from the American Type Culture Collection (ATCC) (Manassas, Virginia, USA) and cultured in Dulbecco's modified Eagle's medium (DMEM) (Corning, Corning, NY, USA) media containing 10% fetal bovine serum (FBS), certified, heat-inactivated, U.S. origin (Gibco, Life Technologies, USA), 1% minimum essential media nonessential amino acids (NEAA, Gibco) and 1% penicillin-streptomycin (PenStrep, Mediatech). Cells were maintained at 37 °C and 5% CO<sub>2</sub> in a humidified incubator.

*Cell Viability Assay:* Cell viability in varying concentrations of the Au@peptide NPs was assessed using PrestoBlue cell viability assay. Human breast adenocarcinoma (MDA-MB-231) and lung fibroblast (IMR-90) cells were seeded in a 96-well flat bottom microplate (BioLite Microwell Plate, Fisher Scientific, Waltham, MA). For IMR-90,  $6.0 \times 10^3$  cells per well were plated, and for MDA-MB-231,  $5.6 \times 10^3$  cells per well were plated in 100  $\mu$ L of DMEM culture media. The cells were allowed to grow for 24 h at 37 °C and 5% CO<sub>2</sub> in a humidified incubator. At confluency, cells were dosed with 0, 1, 2, 5, 10, or 50 nM of Au@peptide NPs (in triplicate). Following the administration of the NPs, cells were incubated for 48 h at 37 °C under 5% CO<sub>2</sub>. After each period of incubation, PrestoBlue (Life Technologies, Carlsbad, CA) was used as an indicator of cellular toxicity; 11  $\mu$ L of PrestoBlue was added to each well and incubated for 1 h at 37 °C under 5% CO<sub>2</sub>. The 96-well plate was then analyzed using a multimode plate-reader BioTek Microplate Reader (BioTek U.S., Winooski, VT) at 560 / 590 nm wavelength. The percentage of surviving cells was calculated as a normalized ratio of the fluorescence intensity between cells treated with AuNPs and media alone.

*Confocal Reflection Imaging:* For all cell imaging experiments,  $8 \times 10^3$  MDA-MB-231 cells or IMR-90 cells were seeded into Nunc™ Lab-Tek™ 8-Chamber Slide with coverslip bottom (Fisher Scientific, USA). After 24 h incubation to allow adhesion, the cells were exposed to 2 nM of NPs for 48 h. Live cell imaging was performed on a Zeiss LSM880 Confocal Microscope equipped with temperature and CO<sub>2</sub> concentration-controlled incubator system. EC Plan Neofluor 10x/0.3 NA (numerical aperture), Plan-Apochromat 20x /0.8 NA and Plan-Apochromat 40x/1.2 NA Water objectives were used. NPs were visualized under confocal reflection mode using 561 nm excitation laser at 1% laser power. In most experiments, confocal reflection mode was combined with brightfield imaging using T-PMT to track the structure and dynamic of the cells.

*TEM*: Human breast adenocarcinoma, MDA-MB-231 cells ( $8 \times 10^3$  cells) were seeded into Nunc™ Lab-Tek™ 8-Chamber Slide (Fisher Scientific, USA) with coverslip bottom. After 24 h of incubation, the cell cultures were exposed to 2 nM of NPs for 1 h, 6 h, 24 h or 48 h and then washed with PBS, fixed with 2% glutaraldehyde and 2% paraformaldehyde solution in 0.1M PBS-sodium cacodylate buffer (50:50, pH 7.0) at 4 °C overnight. In the same chamber slides, cells were post-fixed with 2% osmium tetroxide, stained with 1% uranyl acetate and embedded in Spurr's resin<sup>[69]</sup> and BEEM® Embedding Capsules Size 3 (EMS, USA). The coverslips were removed by briefly dipping the chamber slide into liquid nitrogen. Sections, 85 nm thick, were cut and collected with standard procedures.<sup>[68]</sup> Samples were examined using a JEM-2100 (JEOL) electron microscopes at the City College of New York.

### Supporting Information

Supporting Information is available from the Wiley Online Library or from the author.

### Acknowledgements

We gratefully acknowledge supports from the National Science Foundation, from NSF DMR #1461499 and NSF CREST-IDEALS, #1547830. We thank the NSF for funding of R.V.U. and R.H.H. through grant number CHE 1808143. The research was supported by a grant (2017510, 'Metabolic Nanotechnology') from the United States–Israel Binational Science Foundation (BSF), Jerusalem, Israel. S.O. and R.V.U. also acknowledge funding support from the CUNY-Strathclyde program for R.H.H.'s graduate studies in a collaborative environment. We acknowledge support from the National Institutes of Health (NIH) grant 2SC1GM127278-07A1 (M.C.). R.H.H. would like to thank Scott Mcphee for the training and assistance on lab instruments. We would like to thank Dr. Tong Wang at the Imaging Facility of CUNY Advanced Science Research Center for instrument use (TEM), scientific and technical assistance.

### Conflict of Interest

The authors declare no conflict of interest.

Received: ((will be filled in by the editorial staff))

Revised: ((will be filled in by the editorial staff))

Published online: ((will be filled in by the editorial staff))

## References

- [1] G. M. Whitesides, B. Grzybowski, *Science* **2002**, *295*, 2418.
- [2] S. Zhang, *Nat. Biotechnol.* **2003**, *21*, 1171.
- [3] R. Freeman, M. Han, Z. Álvarez, J. A. Lewis, J. R. Wester, N. Stephanopoulos, M. T. McClendon, C. Lynsky, J. M. Godbe, H. Sangji, E. Luijten, S. I. Stupp, *Science* **2018**, *362*, 808.
- [4] F. Versluis, J. H. van Esch, R. Eelkema, *Adv. Mater.* **2016**, *28*, 4576.
- [5] M. R. Jones, K. D. Osberg, R. J. MacFarlane, M. R. Langille, C. A. Mirkin, *Chem. Rev.* **2011**, *111*, 3736.
- [6] J. Mosquera, I. García, M. Henriksen-Lacey, M. Martínez-Calvo, M. Dhanjani, J. L. Mascareñas, L. M. Liz-Marzán, *ACS Nano* **2020**, *14*, 5382.
- [7] Z. Chu, Y. Han, T. Bian, S. De, P. Král, R. Klajn, *J. Am. Chem. Soc.* **2019**, *141*, 1949.
- [8] M. Grzelczak, J. Vermant, E. M. Furst, L. M. Liz-Marzán, *ACS Nano* **2010**, *4*, 3591.
- [9] C. A. Mirkin, R. L. Letsinger, R. C. Mucic, J. J. Storhoff, *Nature* **1996**, *382*, 607.
- [10] D. Nykypanchuk, M. M. Maye, D. Van Der Lelie, O. Gang, *Nature* **2008**, *451*, 549.
- [11] Y. Kim, R. J. Macfarlane, M. R. Jones, C. A. Mirkin, *Science* **2016**, *351*, 579.
- [12] N. Kim, E. Kim, H. Kim, M. R. Thomas, A. Najer, M. M. Stevens, *Adv. Mater.* **2021**, *33*, DOI 10.1002/adma.202007738.
- [13] M. Grzelczak, L. M. Liz-Marzán, R. Klajn, *Chem. Soc. Rev.* **2019**, *48*, 1342.
- [14] M. Sawczyk, R. Klajn, *J. Am. Chem. Soc.* **2017**, *139*, 17973.
- [15] Y. Shi, D. S. Ferreira, J. Banerjee, A. R. Pickford, H. S. Azevedo, *Biomater. Sci.* **2019**, *7*, 5132.
- [16] R. Chandrawati, M. M. Stevens, *Chem. Commun.* **2014**, *50*, 5431.
- [17] A. Laromaine, L. Koh, M. Murugesan, R. V. Ulijn, M. M. Stevens, *J. Am. Chem. Soc.* **2007**, *129*, 4156.
- [18] C. N. Loynachan, A. P. Soleimany, J. S. Dudani, Y. Lin, A. Najer, A. Bekdemir, Q.

- Chen, S. N. Bhatia, M. M. Stevens, *Nat. Nanotechnol.* **2019**, *14*, 883.
- [19] M. M. Stevens, N. T. Flynn, C. Wang, D. A. Tirrell, R. Langer, *Adv. Mater.* **2004**, *16*, 915.
- [20] M. G. Ryadnov, B. Ceyhan, C. M. Niemeyer, D. N. Woolfson, *J. Am. Chem. Soc.* **2003**, *125*, 9388.
- [21] S. Mokashi-Punekar, A. D. Merg, N. L. Rosi, *J. Am. Chem. Soc.* **2017**, *139*, 15043.
- [22] S. Mokashi-Punekar, S. C. Brooks, C. D. Hogan, N. L. Rosi, *Biochemistry* **2021**, *60*, 1044.
- [23] R. Lévy, N. T. K. Thanh, R. Christopher Doty, I. Hussain, R. J. Nichols, D. J. Schiffrin, M. Brust, D. G. Fernig, *J. Am. Chem. Soc.* **2004**, *126*, 10076.
- [24] A. Salvati, A. S. Pitek, K. Monopoli, Marco P. Prapainop, F. Baldelli Bombelli, D. R. Hristov, P. Kelly, C. Åberg, E. Mahon, K. A. Dawson, *Nat. Nanotechnol.* **2013**, *8*, 137.
- [25] M. P. Monopoli, C. Åberg, A. Salvati, K. A. Dawson, *Nat. Nanotechnol.* **2012**, *7*, 779.
- [26] M. Borkowska, M. Siek, D. V. Kolygina, Y. I. Sobolev, S. Lach, S. Kumar, Y. K. Cho, K. Kandere-Grzybowska, B. A. Grzybowski, *Nat. Nanotechnol.* **2020**, *15*, 331.
- [27] X. Liu, Y. Chen, H. Li, N. Huang, Q. Jin, K. Ren, J. Ji, *ACS Nano* **2013**, *7*, 6244.
- [28] X. Liu, H. Li, Q. Jin, J. Ji, *Small* **2014**, *10*, 4230.
- [29] D. Li, B. Kumari, J. M. Makabenta, A. Gupta, V. Rotello, *Nanoscale* **2019**, *11*, 22172.
- [30] K. Saha, S. S. Agasti, C. Kim, X. Li, V. M. Rotello, *Chem. Rev.* **2012**, *112*, 2739.
- [31] S. Laing, L. E. Jamieson, K. Faulds, D. Graham, *Nat. Rev. Chem.* **2017**, *1*, 0060.
- [32] J. K. Sahoo, N. M. S. Sirimuthu, A. Canning, M. Zelzer, D. Graham, R. V. Ulijn, *Chem. Commun.* **2016**, *52*, 4698.
- [33] D. A. Giljohann, D. S. Seferos, W. L. Daniel, M. D. Massich, P. C. Patel, C. A. Mirkin, *Angew. Chemie - Int. Ed.* **2010**, *49*, 3280.
- [34] S. Wang, S. S. Park, C. T. Buru, H. Lin, P.-C. Chen, E. W. Roth, O. K. Farha, C. A. Mirkin, *Nat. Commun.* **2020**, 2495.

- [35] D. Kalafatovic, M. Nobis, N. Javid, P. W. J. M. Frederix, K. I. Anderson, B. R. Saunders, R. V. Ulijn, *Biomater. Sci.* **2015**, *3*, 246.
- [36] A. R. Farina, A. R. Mackay, *Cancers* **2014**, *6*, 240.
- [37] D. Kalafatovic, M. Nobis, J. Son, K. I. Anderson, R. V. Ulijn, *Biomaterials* **2016**, *98*, 192.
- [38] W. Ke, J. Li, K. Zhao, Z. Zha, Y. Han, Y. Wang, W. Yin, P. Zhang, Z. Ge, *Biomacromolecules* **2016**, *17*, 3268.
- [39] T. Ji, S. Li, Y. Zhang, J. Lang, Y. Ding, X. Zhao, R. Zhao, Y. Li, J. Shi, J. Hao, Y. Zhao, G. Nie, *ACS Appl. Mater. Interfaces* **2016**, *8*, 3438.
- [40] N. D. Rawlings, A. J. Barrett, R. Finn, *Nucleic Acids Res.* **2016**, *44*, D343.
- [41] A. Jaiswal, A. Chhabra, U. Malhotra, S. Kohli, V. R. Vibha Rani, *Bioinformatics* **2011**, *6*, 23.
- [42] J. Son, D. Kalafatovic, M. Kumar, B. Yoo, M. A. Cornejo, M. Contel, R. V. Ulijn, *ACS Nano* **2019**, *13*, 1555.
- [43] M. D. Porter, T. B. Bright, D. L. Allara, C. E. Chidsey, *J. Am. Chem. Soc.* **1987**, *109*, 3559.
- [44] S. Zhanga, Y. Lin, M. Altman, M. Lässle, H. Nugent, F. Frankel, D. A. Lauffenburger, G. M. Whitesides, A. Rich, *Biomaterials* **1999**, *20*, 1213.
- [45] M. Rolli, E. Fransvea, J. Pilch, A. Saven, B. Felding-Habermann, *Proc. Natl. Acad. Sci. U. S. A.* **2003**, *100*, 9482.
- [46] F. Danhier, A. Le Breton, V. Préat, *Mol. Pharm.* **2012**, *9*, 2961.
- [47] J. N. Roberts, J. K. Sahoo, L. E. McNamara, K. V. Burgess, J. Yang, E. V. Alakpa, H. J. Anderson, J. Hay, L. A. Turner, S. J. Yarwood, M. Zelzer, R. O. C. Oreffo, R. V. Ulijn, M. J. Dalby, *ACS Nano* **2016**, *10*, 6667.
- [48] Y. Huang, J. Shi, D. Yuan, N. Zhou, B. Xu, *Biopolymers* **2013**, *100*, 790-795.
- [49] S.-Y. Lin, Y.-T. Tsai, C.-C. Chen, C.-M. Lin, C. Chen, *J. Phys. Chem. B* **2004**, *108*,

- 2134.
- [50] R. G. Acres, V. Feyer, N. Tsud, E. Carlino, K. C. Prince, *J. Phys. Chem. C* **2014**, *118*, 10481.
- [51] H. M. Zakaria, A. Shah, M. Konieczny, J. A. Hoffmann, A. J. Nijdam, M. E. Reeves, *Langmuir* **2013**, *29*, 7661.
- [52] F. X. Zhang, L. Han, L. B. Israel, J. G. Daras, M. M. Maye, N. K. Ly, C. J. Zhong, *Analyst* **2002**, *127*, 462.
- [53] H. Hinterwirth, S. Kappel, T. Waitz, T. Prohaska, W. Lindner, M. Lämmerhofer, *ACS Nano* **2013**, *7*, 1129.
- [54] A. B. Grommet, M. Feller, R. Klajn, *Nat. Nanotechnol.* **2020**, *15*, 256.
- [55] J. N. Roberts, J. K. Sahoo, L. E. McNamara, K. V. Burgess, J. Yang, E. V. Alakpa, H. J. Anderson, J. Hay, L. A. Turner, S. J. Yarwood, M. Zelzer, R. O. C. Oreffo, R. V. Ulijn, M. J. Dalby, *ACS Nano* **2016**, *10*, 6667.
- [56] M. Mahmoudi, K. Azadmanesh, M. A. Shokrgozar, W. S. Journey, S. Laurent, *Chem. Rev.* **2011**, *111*, 3407.
- [57] Y. X. Li, H. B. Pang, *J. Control. Release* **2021**, *329*, 1222.
- [58] M. C. Kerr, R. D. Teasdale, *Traffic* **2009**, *10*, 364.
- [59] J. Z. Rappoport, S. M. Simon, *J. Cell Sci.* **2003**, *116*, 847.
- [60] K. Yang, Y. Liu, Y. Wang, Q. Ren, H. Guo, J. B. Matson, X. Chen, Z. Nie, *Biomaterials* **2019**, *223*, 119460.
- [61] A. Kapara, V. Brunton, D. Graham, K. Faulds, *Chem. Sci.* **2020**, *11*, 5819.
- [62] Y. Tian, Y. Zhang, Z. Teng, W. Tian, S. Luo, X. Kong, X. Su, Y. Tang, S. Wang, G. Lu, *ACS Appl. Mater. Interfaces* **2017**, *9*, 2114.
- [63] J. Langer, D. J. de Aberasturi, J. Aizpurua, R. A. Alvarez-Puebla, B. Auguie, J. J. Baumberg, G. C. Bazan, S. E. J. Bell, A. Boisen, A. G. Brolo, J. Choo, D. Cialla-May, V. Deckert, L. Fabris, K. Faulds, F. Javier García de Abajo, R. Goodacre, D. Graham,

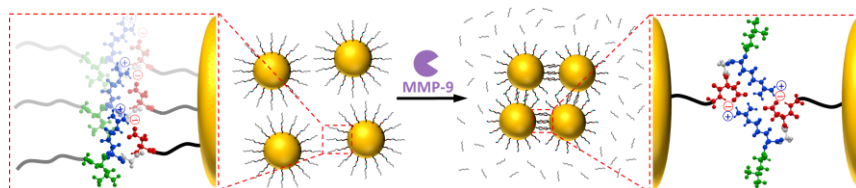
- A. J. Haes, C. L. Haynes, C. Huck, T. Itoh, M. Käll, J. Kneipp, N. A. Kotov, H. Kuang, E. C. Le Ru, H. K. Lee, J. F. Li, X. Y. Ling, S. A. Maier, T. Mayerhöfer, M. Moskovits, K. Murakoshi, J. M. Nam, S. Nie, Y. Ozaki, I. Pastoriza-Santos, J. Perez-Juste, J. Popp, A. Pucci, S. Reich, B. Ren, G. C. Schatz, T. Shegai, S. Schlücker, L. L. Tay, K. George Thomas, Z. Q. Tian, R. P. van Duyne, T. Vo-Dinh, Y. Wang, K. A. Willets, C. Xu, H. Xu, Y. Xu, Y. S. Yamamoto, B. Zhao, L. M. Liz-Marzán, *ACS Nano* **2020**, *14*, 28.
- [64] M. Ben Haddada, M. Salmain, S. Boujday, *Sensors Actuators, B Chem.* **2018**, *255*, 1604.
- [65] T. Ueland, J. Holter, A. Holten, K. Muller, A. Lind, G. Bekken, S. Dudman, P. Aukrust, A. Dyrhol-Riise, L. Heggelund, *J. Infect.* **2020**, *81*, e41.
- [66] L. E. Valenti, M. B. Paci, C. P. De Pauli, C. E. Giacomelli, *Anal. Biochem.* **2011**, *410*, 118.
- [67] J. Turkevich, P. C. Stevenson, J. Hillier, *Discuss. Faraday Soc.* **1951**, *11*, 55.
- [68] G. Frens, *Nat. Phys. Sci.* **1973**, *242*, 344.
- [69] A. R. Spurr, *J Ultrastruct Res.* **1969**, *26*, 31.
- [70] J. J. Bozzola, L. D. Russell, *Electron Microscopy: Principles and Techniques for Biologists*, 2nd ed., Jones & Bartlett Learning, **1999**.

An enzyme-activated assembly of AuNPs using the zwitterionic peptide, LRGD, as a self-complementary, electrostatic binding moiety is illustrated. PEGylated peptide ligands containing the LRGD sequence are immobilized on the AuNPs. Cancer-specific enzymes, matrix metalloproteinase-9 (MMP-9), cleave the peptide ligands and subsequently reveal the LRGD moieties that promote multivalent, electrostatic interactions, leading to the assembly of the AuNPs.

R. H. Huang, N. Nayeem, Y. He, J. Morales, D. Graham, R. Klajn, M. Contel, S. O'Brien, and R. V. Ulijn\*

### Self-Complementary Zwitterionic Peptides Direct Nanoparticle Assembly and Enable Enzymatic Selection of Endocytic Pathways

ToC figure



## Supporting Information

**Programmable Nanoparticle Assembly and Endocytic Pathways using MMP-responsive, Charge-Complementary Peptides**

Richard H. Huang, Nazia Nayeem, Ye He, Jorge Morales, Duncan Graham, Rafal Klajn, Maria Contel, Stephen O'Brien, and Rein V. Ulijn\*

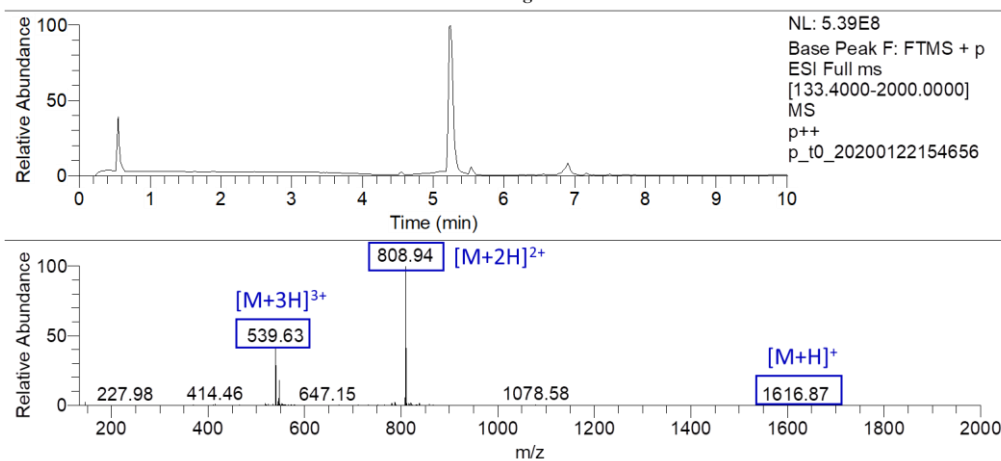
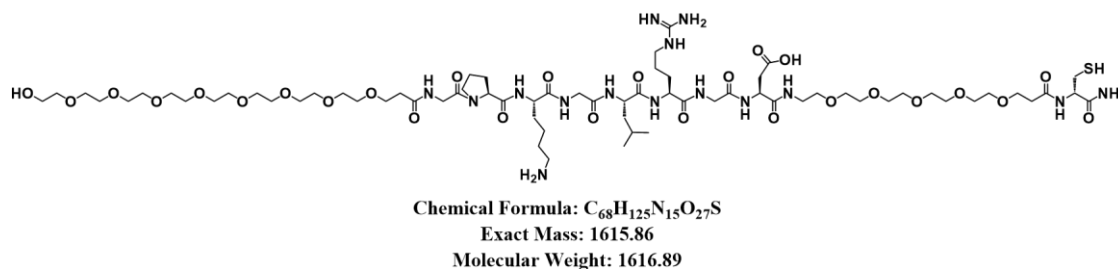
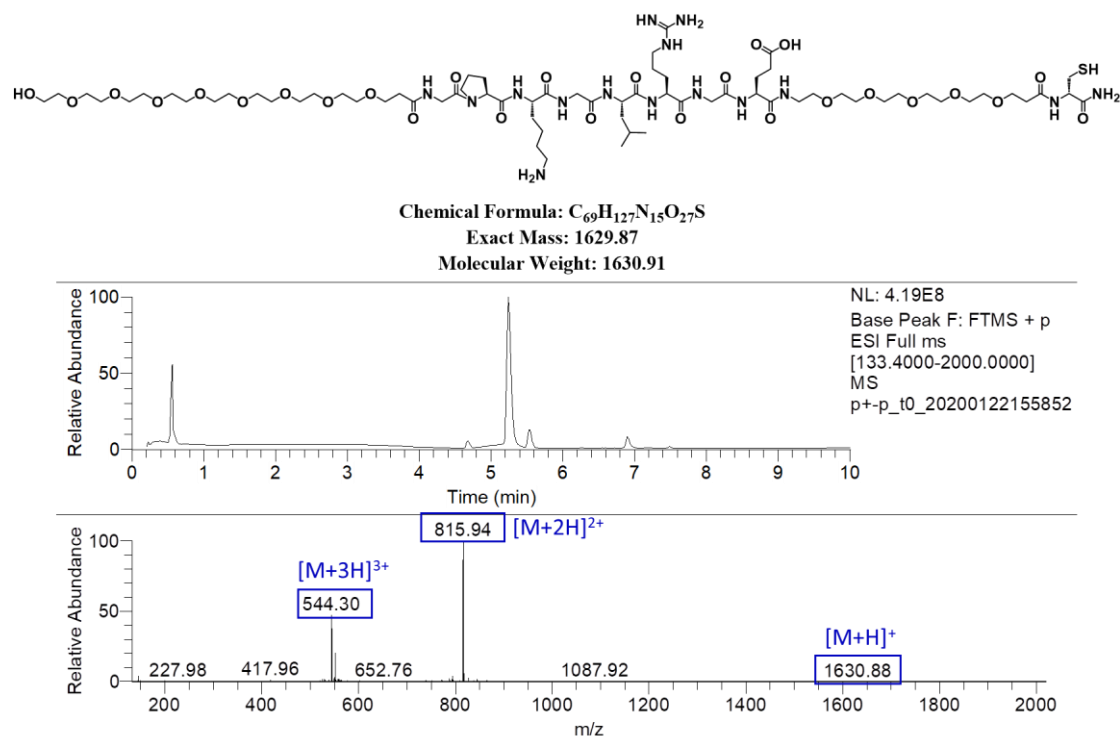
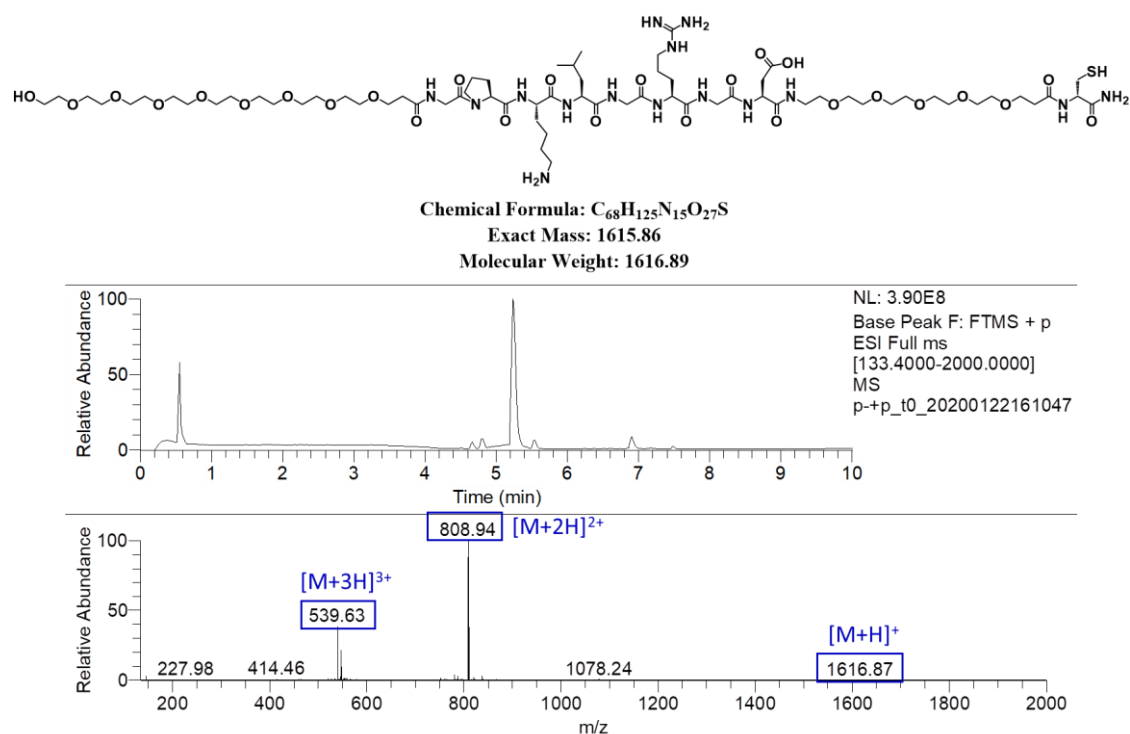


Figure S1A. Structural details and LCMS spectra of GLD.



**Figure S1B.** Structural details and LCMS spectra of **GLE**.



**Figure S1C.** Structural details and LCMS spectra of **LGD**.

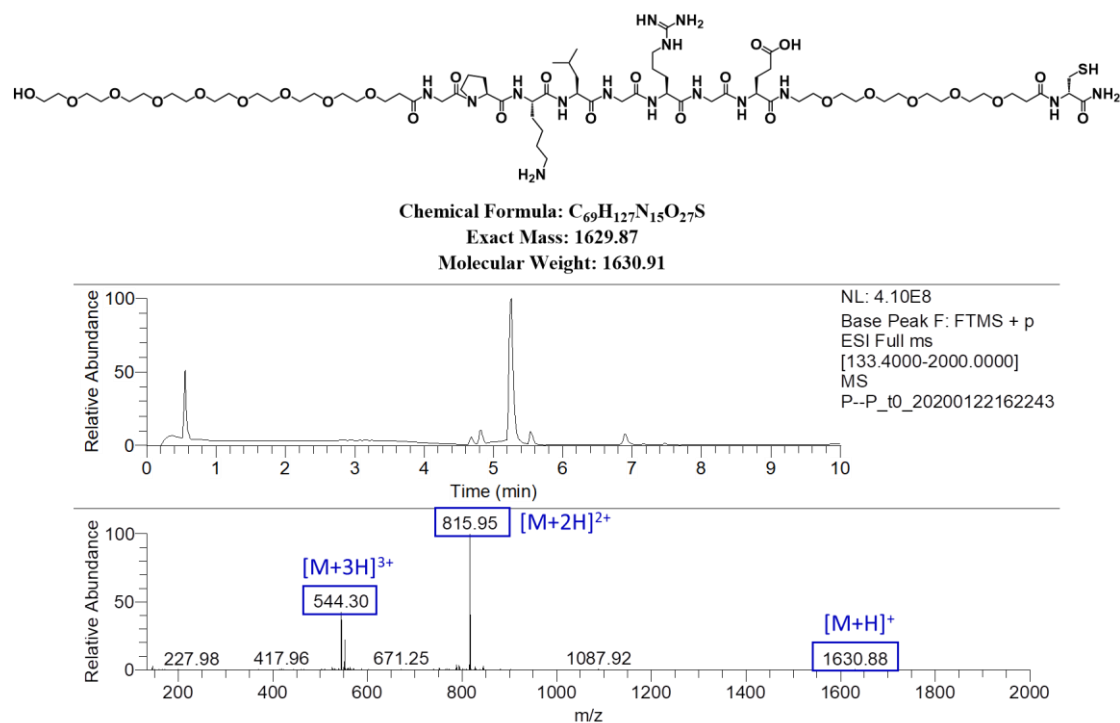


Figure S1D. Structural details and LCMS spectra of LGE.

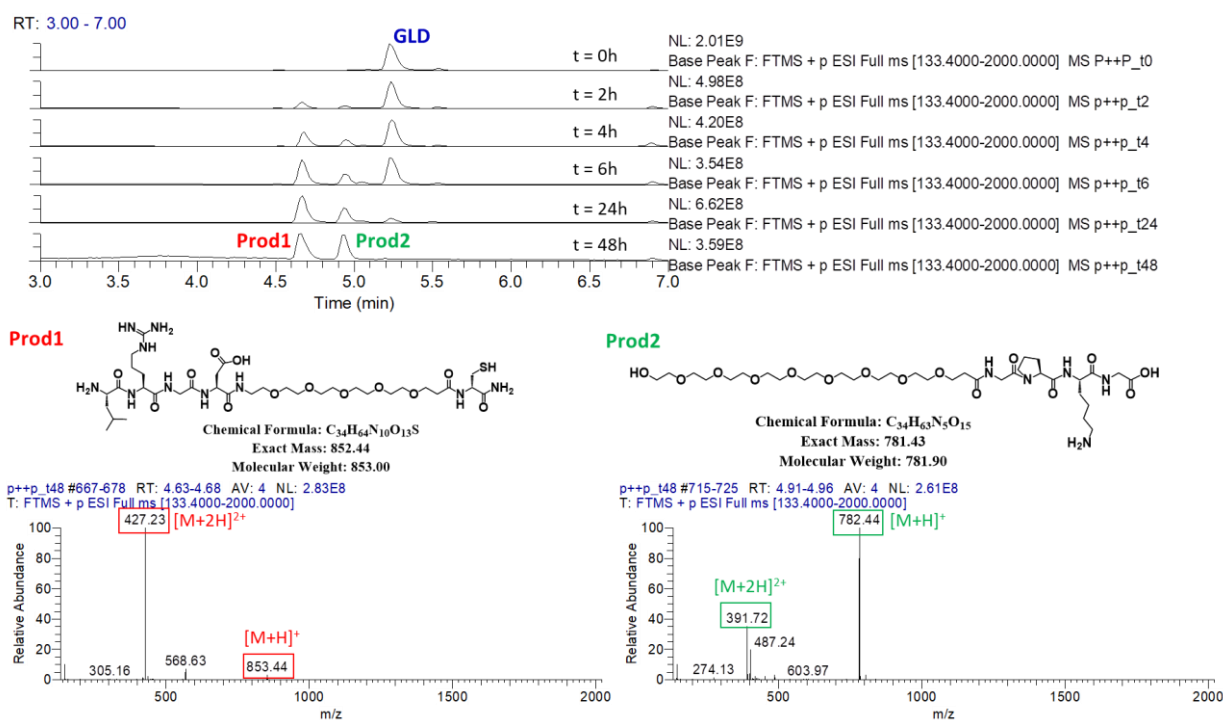
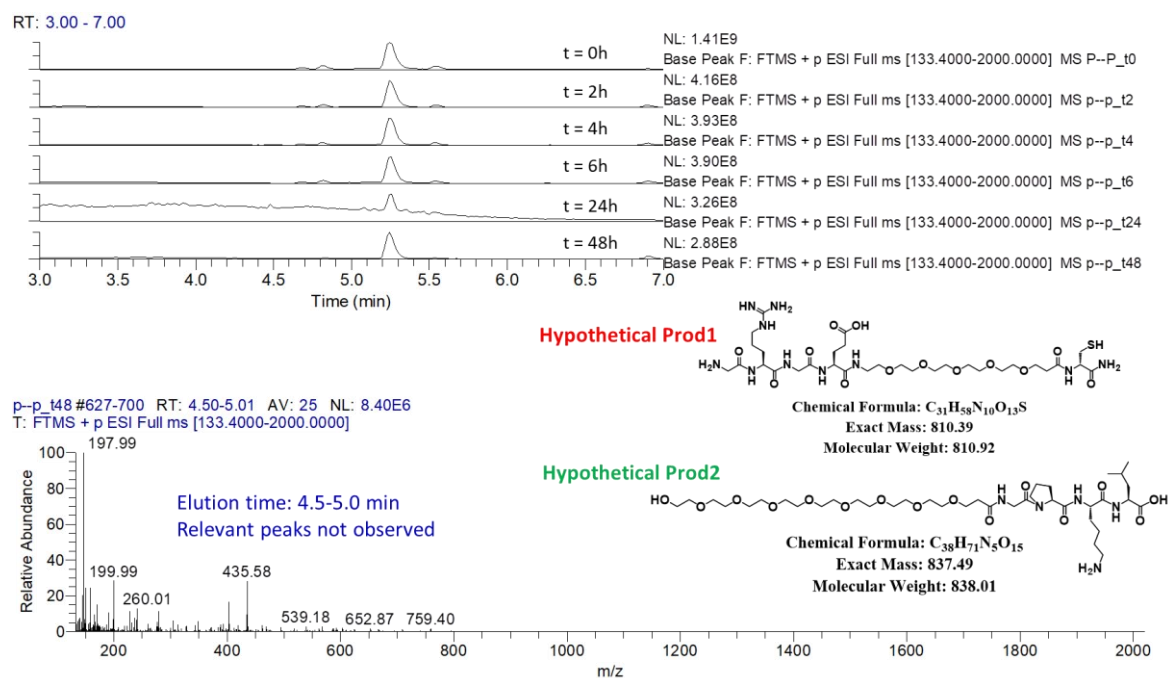
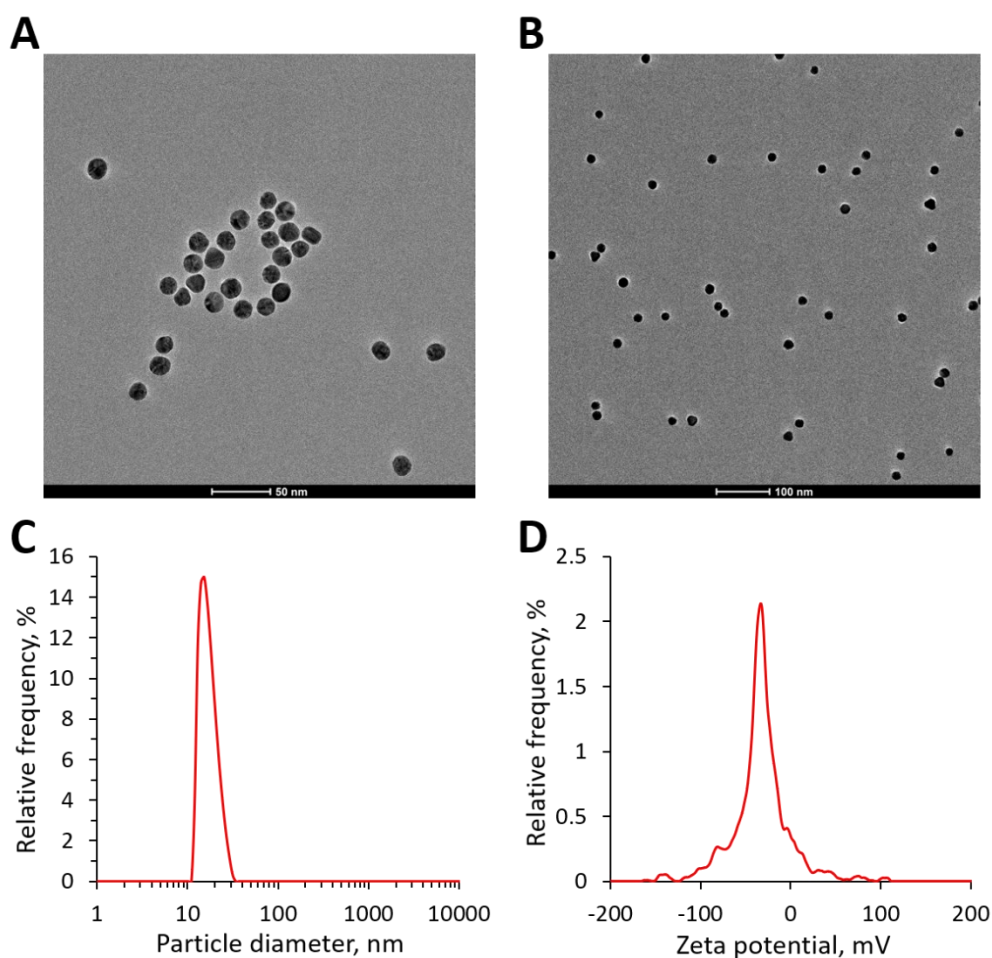


Figure S2A. LCMS characterization of GLD (1 mM) incubated with MMP-9 (100 ng/mL) over 48 hours.





**Figure S2D.** LCMS characterization of LGE (1 mM) incubated with MMP-9 (100 ng/mL) over 48 hours. MS peaks for the hypothetical enzymatic fragments were not detected.



**Figure S3.** Characterization of AuNPs synthesized by the citrate reduction method. (A) and (B) TEM images of as-synthesized AuNPs. (C) Hydrodynamic diameter of AuNPs by DLS;  $17.5 \pm 0.5$  nm. (D) Zeta-potential measurement;  $-33.8 \pm 2.9$  mV.

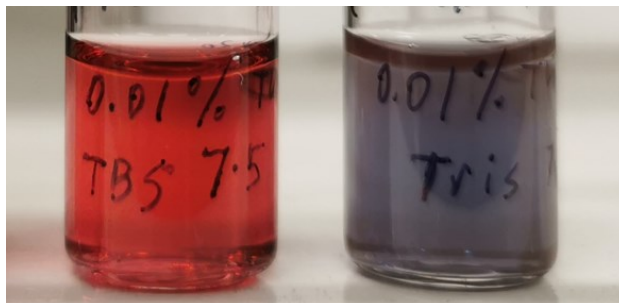


**Figure S4.** Photographs of Au@LA (left) and Au@Citrate (right) after redispersion in TBS buffer at pH 7.5, indicating the successful coating of LA onto the Au surface.

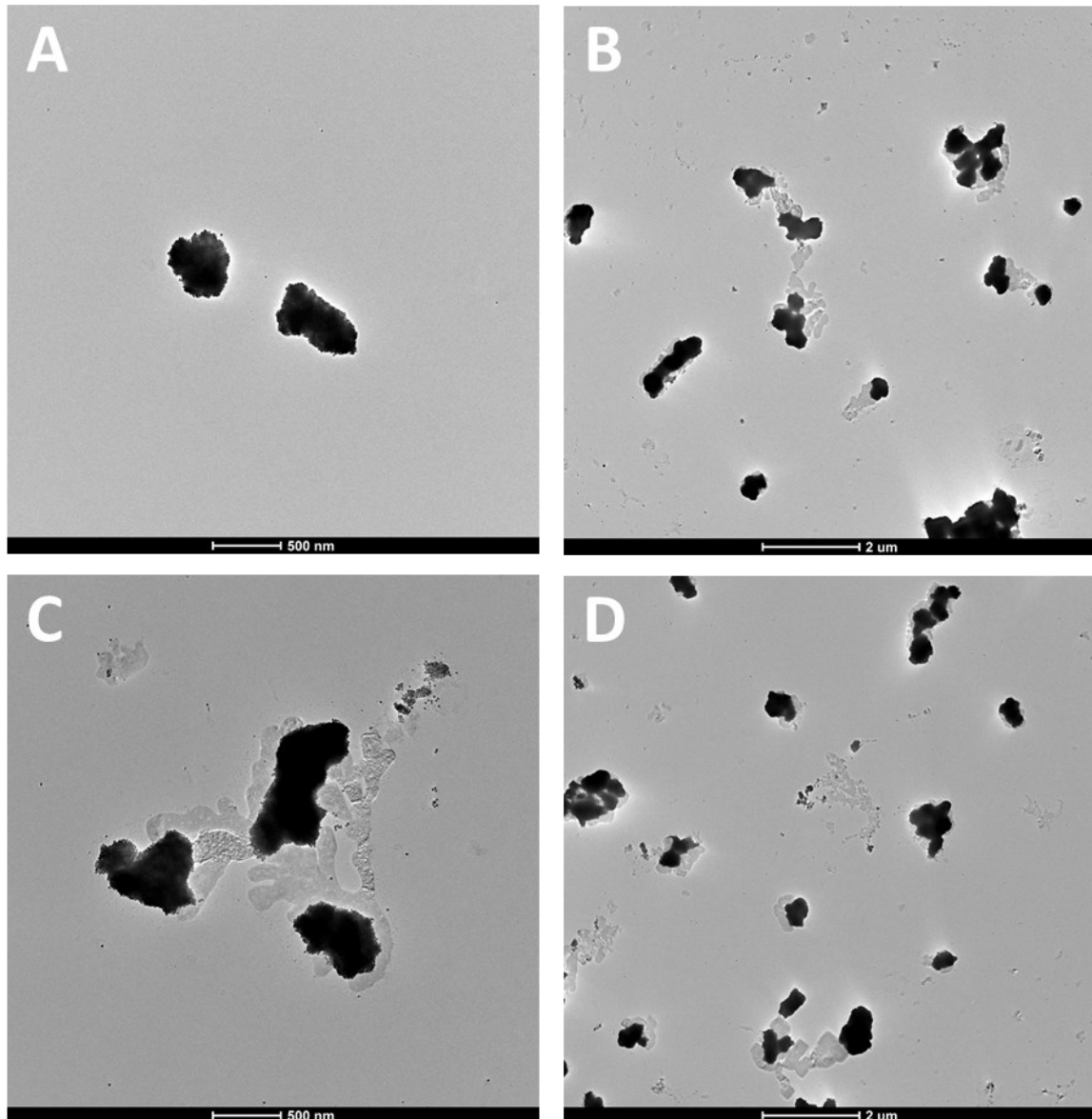


**Figure S5.** Additional TEM images of Au@GLD (A, B) and Au@GLE (C, D) after incubation with MMP-9 for 48 hours.

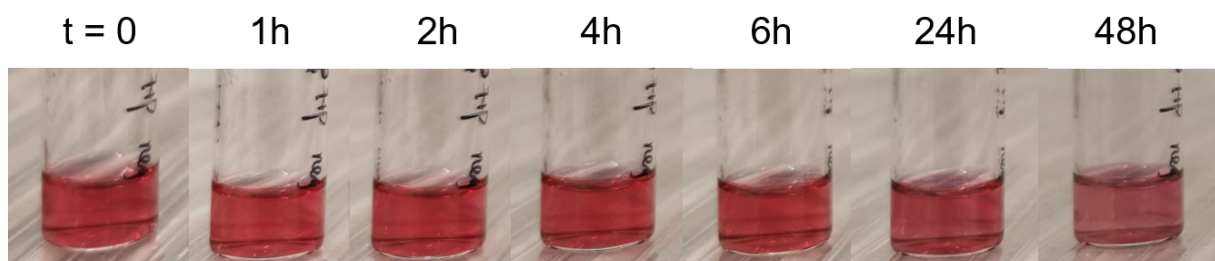


**Figure S6.** Photographs of Au@GLD functionalized with PEG-2000 (Au@GLD-PEG-2000) incubated with 100 ng/mL of MMP-9 at 37 °C and pH 7.4 over 48 hours. The color of the solution remained bright-red in the first 24 hours and turned slightly purple-red at t = 48 hours,

indicating either a slow cleavage rate of the peptides functionalized with PEG-2000 or efficient stabilization of AuNPs by PEG-2000 even after cleavage.

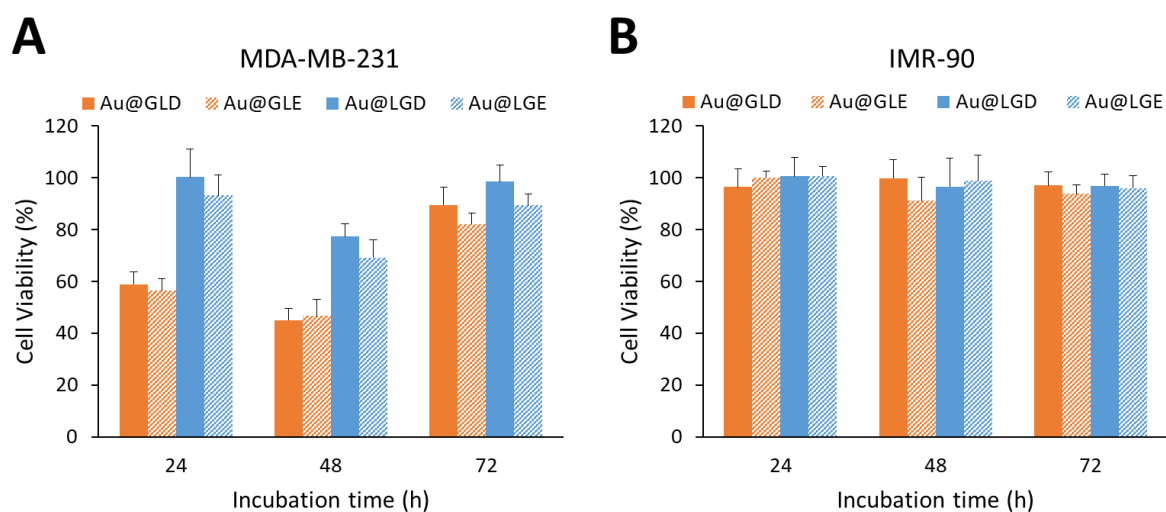


**Figure S7.** Cell viability of MDA-MB-231 triple negative breast cancer cells (A) and IMR-90 normal lung fibroblast cells (B) following 24, 48, and 72 hours of incubation with 1 nM of peptide-functionalized NPs. Error bars, mean  $\pm$  SD. The viability of MDA-MB-231 first decreased from 24 to 48 hours due to cytotoxicity of the internalized NP aggregates, and increased from 48 to 72 hours, likely due to cell recovery and continued proliferation of unaffected cells.

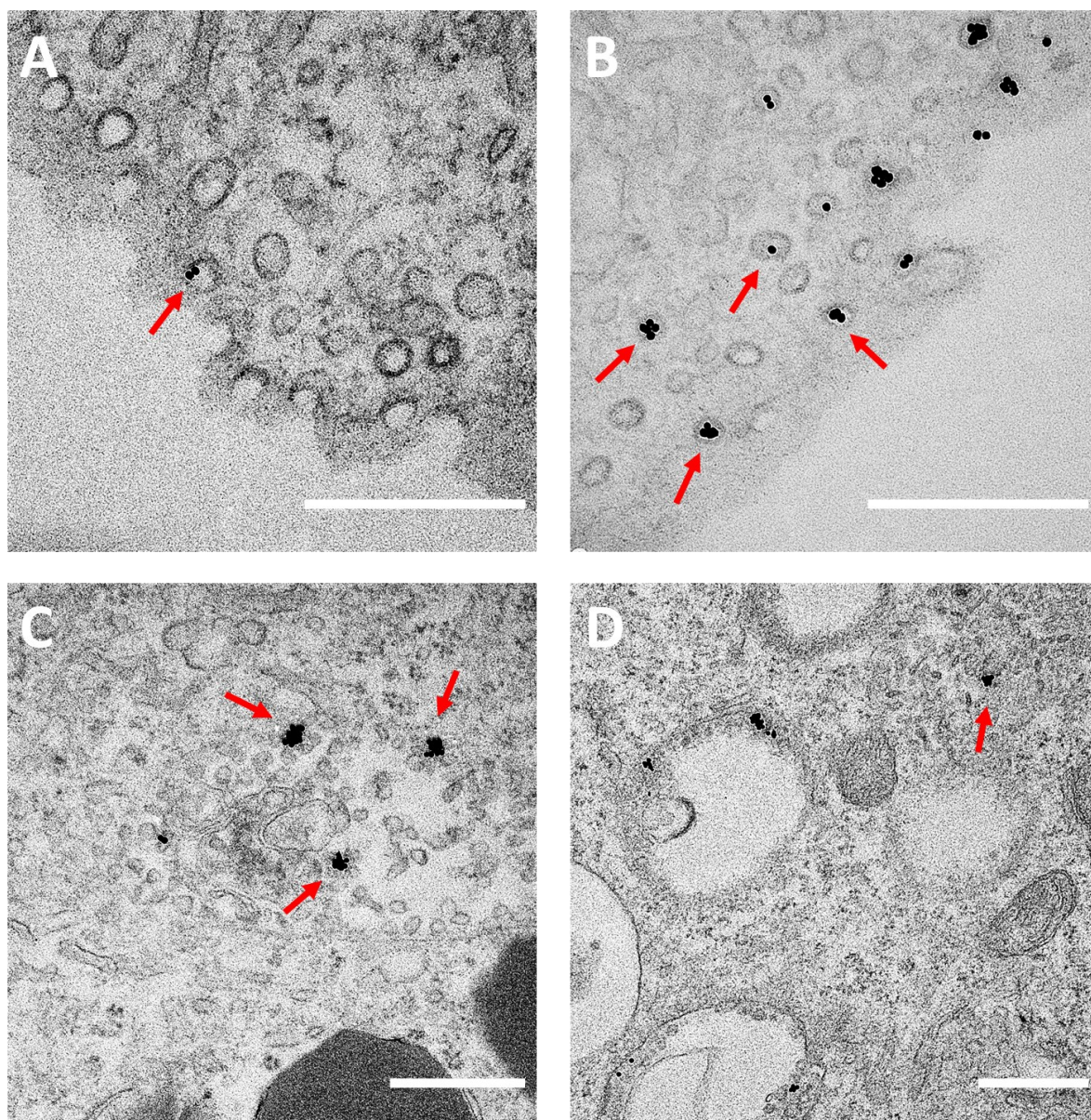


**Figure S8.** TEM images of Au@LGD NPs (highlighted by red arrows) in MDA-MB-231 cells in vesicles (A, B) and in cytoplasm (C, D). Scale bars, 500 nm.

### Supporting Experimental Section

**Liquid chromatography–mass spectrometry (LCMS).** 50  $\mu\text{L}$  of the enzyme reaction solution (or peptide-only solution at  $t = 0$ ) was taken out at different time points and directly added to 450  $\mu\text{L}$  of 20% acetonitrile in water containing 0.1% formic acid (FA). Samples were analyzed on an LCMS system comprising a Thermo Fisher Vanquish LC system coupled to an electro spray ionization (ESI) mass spectrometer. Samples were injected onto

an a Phenomenex Luna100 Å 5 µm 50x2 mm C18(2) column using a gradient of 2–50% acetonitrile in water (0.1% FA) at a flow rate of 0.4 µL/min over 10 min followed by a 2-minute wash step with 95% acetonitrile.

**Hydrodynamic diameter and ζ-potential measurements.** The hydrodynamic diameter and surface charge were recorded using an Anton Paar Litesizer 500 Particle Analyzer. For the particle size measurements, a quartz cuvette was used to hold 1 mL of AuNPs or Au@peptides aqueous solution. The volume weighted size distribution peak values were used to report the hydrodynamic diameters. For the ζ-potential measurements, the AuNPs or Au@peptides NPs were prepared in 10 mM of sodium phosphate buffer (pH 7.0) and 0.3 mL of each sample was injected into an Omega cuvette. Measurements were made at 25 °C using Smoluchowski approximation with a maximal voltage of 200 V.

**Transmission electron microscopy (TEM).** The TEM images of AuNPs were taken on FEI Titan Themis 200 kV TEM. AuNPs, Au@peptide NPs before cleavage, and Au@peptide NPs after cleavage were prepared in Milli-Q water, and 5 µL of the solution was drop casted on a carbon film grid (300 mesh, copper) and dried completely.

**UV-Vis spectroscopy.** The UV-Vis absorption spectra of the AuNPs were recorded on JASCO V-660 UV-Vis spectrophotometer using quartz cuvettes with 1 cm path length. Scans were recorded in the range 300–900 nm at a scan speed of 1000 nm/min and 0.5 nm data interval.